Chemistry–A European Journal
Research Article
doi.org/10.1002/chem.202203187
Chemistry Europe
European Chemical Societies Publishing
www.chemeurj.org

Controlled Formation of Porous 2D Lattices from C_3-symmetric Ph_6–Me-Tribenzotriquinacene-OAc_3

Sinem Toksabay,[a] Markus Leisegang,*[b] Andreas Christ,[b] Patrick Härtl,[b] Johannes Krebs,[c] Todd B. Marder,[c] Soumyajyoti Haldar,[d] Stefan Heinze,[d] Matthias Bode,[b, e] and Anke Krueger*[a, f]

Abstract: The on-surface self-assembly of molecules to form holey nanographenes is a promising approach to control the properties of the resulting 2D lattice. Usually, planar molecules are utilized to prepare flat, structurally confined molecular layers, with only a few recent examples of warped precursors. However, control of the superstructures is limited thus far. Herein, we report the temperature-controlled self-assembly of a bowl-shaped, acetylated C_3-symmetric hexaphenyltribenzotriquinacene derivative on Cu(111). Combining scanning tunneling microscopy (STM) and density functional theory (DFT) confirms the formation of highly differing arrangements starting with π-stacked bowl-to-bowl dimers at low coverage at room temperature via chiral honeycomb structures, an intermediate trigonal superstructure, followed by a fully carbon-based, flattened hexagonal superstructure formed by on-surface deacetylation, which is proposed as a precursor for holey graphene networks with unique defect structures.

Introduction

The self-assembly of molecules on substrates can lead to extended networks with higher-order structures.[1–3] Such nano- or even microscale layers have been proposed for numerous applications in sensing, electronics, catalysis, surface structuring, etc.[4,5] Their actual structures and properties are governed by the nature and orientation of the substrate as well as the structural properties of the assembled molecules.[5] As the interaction between substrate and adsorbate as well as intermolecular interactions are typically based on rather weak forces such as π-π interactions, dispersion forces, or hydrogen bonds in the presence of polar groups,[6] one viable strategy might be to steer the molecular orientation by external stimuli such that they form specific 2D lattices suitable for the desired superstructures.[7] Examples include graphene nanoribbons, flake-like nanographenes as well as zigzag and holey structures. Perfectly flat, structurally-confined nanographenes have been produced on surfaces using self-assembly and on-surface reactions of mainly planar aromatic precursor molecules.[8–12] Warped precursors, such as extended rubicenes, have been used recently to open the path to defective nanographenes,[13] highly sought after for electronic applications. In another study, Fasel and coworkers observed the formation of extended homochiral honeycomb networks of a warped nanographene adsorbate and elucidated the contribution of π-π and C–H-π interactions.[14] Highly symmetric and ordered 2D layers of molecules with a threefold symmetry have been observed recently in different studies.[43] However, control of the formation of different structures from the same C_3-symmetric molecule has rarely been observed. For example, Herges and colleagues reported on the coverage-controlled superstructure formation for C_3-symmetric molecules as-

[a] Dr. S. Toksabay, Prof. Dr. A. Krueger
Institute for Organic Chemistry
Julius-Maximilians-Universität Würzburg
Am Hubland, 97074 Würzburg (Germany)
E-mail: anke.krueger@oc.uni-stuttgart.de

[b] Dr. M. Leisegang, A. Christ, P. Härtl, Prof. Dr. M. Bode
Physikalisches Institut
Experimentelle Physik II
Julius-Maximilians-Universität Würzburg
Am Hubland, 97074 Würzburg (Germany)
E-mail: markus.leisegang@physik.uni-wuerzburg.de

[c] Dr. J. Krebs, Prof. Dr. T. B. Marder
Institute for Inorganic Chemistry and
Institute for Sustainable Chemistry & Catalysis with Boron
Julius-Maximilians-Universität Würzburg
Am Hubland, 97074 Würzburg (Germany)

[d] Dr. S. Haldar, Prof. Dr. S. Heinze
Institute of Theoretical Physics and Astrophysics
University of Kiel
Leibnizstrasse 15, 24098 Kiel (Germany)

[e] Prof. Dr. M. Bode
Wilhelm Conrad Röntgen-Center for Complex Material Systems (RCCM)
Julius-Maximilians-Universität Würzburg
Am Hubland, 97074 Würzburg (Germany)

[f] Prof. Dr. A. Krueger
Institute of Organic Chemistry
University of Stuttgart
Pfaffenwaldring 55, 70569 Stuttgart (Germany)

Supporting information for this article is available on the WWW under https://doi.org/10.1002/chem.202203187

sembled on Au and Ag substrates.[15] They observed the formation of honeycomb or hexagonal assembly structures from the cone-shaped precursors, depending on the coverage with methyl trioxatriangulenium, which led to lattices with different pore size. However, only a few examples of the controlled creation of multiple defined structures by a single organic molecule in response to external stimuli have been reported to date.

Herein, we report that the temperature-controlled self-assembly of a C_3-symmetric hexaphenyltribenzotriquinacene derivative carrying an apical methyl group on a copper substrate leads to a surprising variety of lattice structures. The gradual cleavage of thermally labile groups at elevated temperatures promotes the formation of entirely carbon-based 2D lattices with increasing density and a defined porosity.

Tribenzotriquinacenes (TBTQs) have recently come into focus as model compounds for highly curved, defective graphene structures[16] and are also being investigated as building blocks for highly porous 3D organic frameworks.[17,18] TBTQs can be functionalized in different positions leading to derivatives with functional moieties for sensing, covalent assembly, or molecular recognition.[19–22] The assembly of simple TBTQs has been studied both in crystals[23–25] and on surfaces.[26] On a metal surface, the arrangement of TBTQ and Me-TBTQ was governed by the surface coverage, and showed hexagonal patterns and honeycomb structures. However, we observed that the interaction between the substrate and the molecules was rather weak. Further arylation of TBTQ and introduction of thermally cleavable leaving groups are proposed to promote self-assembly and control of the deposition process. We thus synthesized triacetyl methyl hexaphenyl-TBTQ (**1**) in order to investigate the self-assembly of this chiral, expanded TBTQ, and investigated its behavior upon deposition on a highly defined metal substrate at different temperatures.

Results and Discussion

Synthesis and characterization of Ph_6–Me-TBTQ-OAc_3 (1)

The synthesis of acetylated hexaphenyl-functionalized methyl tribenzotriquinacene (Ph_6Me-TBTQ-OAc_3) was achieved in a nine-step process, as shown in Figure 1a. The intermediate Me-TBTQ **2** was obtained using a previously reported procedure.[27] The bromination of **2** was performed using a Wohl-Ziegler reaction, according to a procedure by Beaudoin et al.,[28] followed by substitution of Br by OH groups and the iodination of the aromatic rings of the TBTQ.[29]

The acetyl groups were introduced by treatment with acetic anhydride and DMAP, adapting a reported protocol.[30] Subsequently, Ph_6–Me-TBTQ-OAc_3 (**1**) was synthesized using a Suzuki-Miyaura cross-coupling reaction between hexaiodo-TBTQ **4** and phenylboronic acid with a yield of 80%. For experimental details and spectroscopic characterization, see the Supporting Information. Single crystals of **1** were analyzed by X-ray diffraction. As shown in Figure 1b, the C_{3v}-symmetric molecules exhibit a bowl shape, which is in good agreement with previous studies on TBTQ molecules.[23–26] In the crystal, these bowls face each other in a bowl-to-bowl arrangement, thus creating dimers in the lattice. The top view in Figure 1c reveals that the six phenyl rings form an alternating pattern of in-plane and out-of-plane orientations, allowing for enantiomers with opposite handedness (for details see the Supporting Information). The acetyl groups were introduced in the bay positions of the triquinacene core

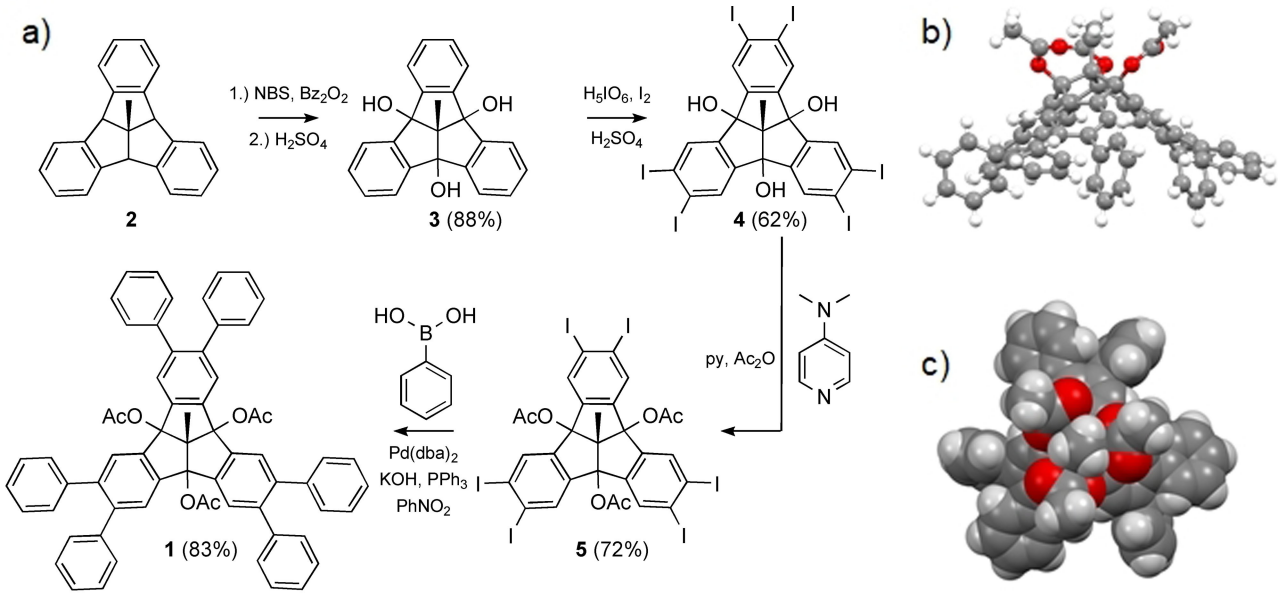

Figure 1. a) Synthetic route to Ph_6–Me-TBTQ-OAc_3 (**1**) and molecular structure of **1** from single-crystal X-ray diffraction b): side view, c): top view.

as thermally labile leaving groups to allow for cleavage at elevated temperatures.

STM experiments

First, a small amount of the evaporator loaded species **1** was deposited on a clean Cu(111) surface. As can be seen in the topography in Figure 2a, the molecules tend to adsorb on step edges of the substrate, indicating a high mobility at room temperature. On the terraces, clusters with a dumbbell shape appear as the dominant form, as shown in the enlarged scan in Figure 2b. STM-induced molecule manipulation allows decomposition of the clusters into two single objects, c.f. Figure 2c–e. This unambiguously shows that each protrusion of the dumbbell depicts one single molecule. The orientation of these dimers is guided by the $\langle 2\bar{1}\bar{1}\rangle$ directions of the substrate, as highlighted by dashed lines in Figure 2b). Occasional deviations of the dimer orientation from the ideal crystal direction might be induced by different adsorption sites of the molecules with respect to the surface lattice.

The height profile in Figure 2g, taken along the dashed line in Figure 2f, reveals a corrugation of ≈300 pm, in good agreement with the diameter of the triquinacene core. Based on these observations, and in accordance with the X-ray crystal structure, we conclude that the molecules are arranged bowl-to-bowl in dimers with an inter-dimer distance of $d_{di=}(1.3\pm0.2)$ nm, as shown in Figure 2f by true-to-scale models. The height profile reveals that the molecules are compressed along the surface normal, thereby significantly reducing the bowl diameter as compared to the lattice parameters in the single crystal (see the Supporting Information), while also indicating the desymmetrization of the molecular structure by the loss of one acetyl group. The latter is supported by mass spectrometry, where the cleavage of one acetyl group is observed as the most prominent process

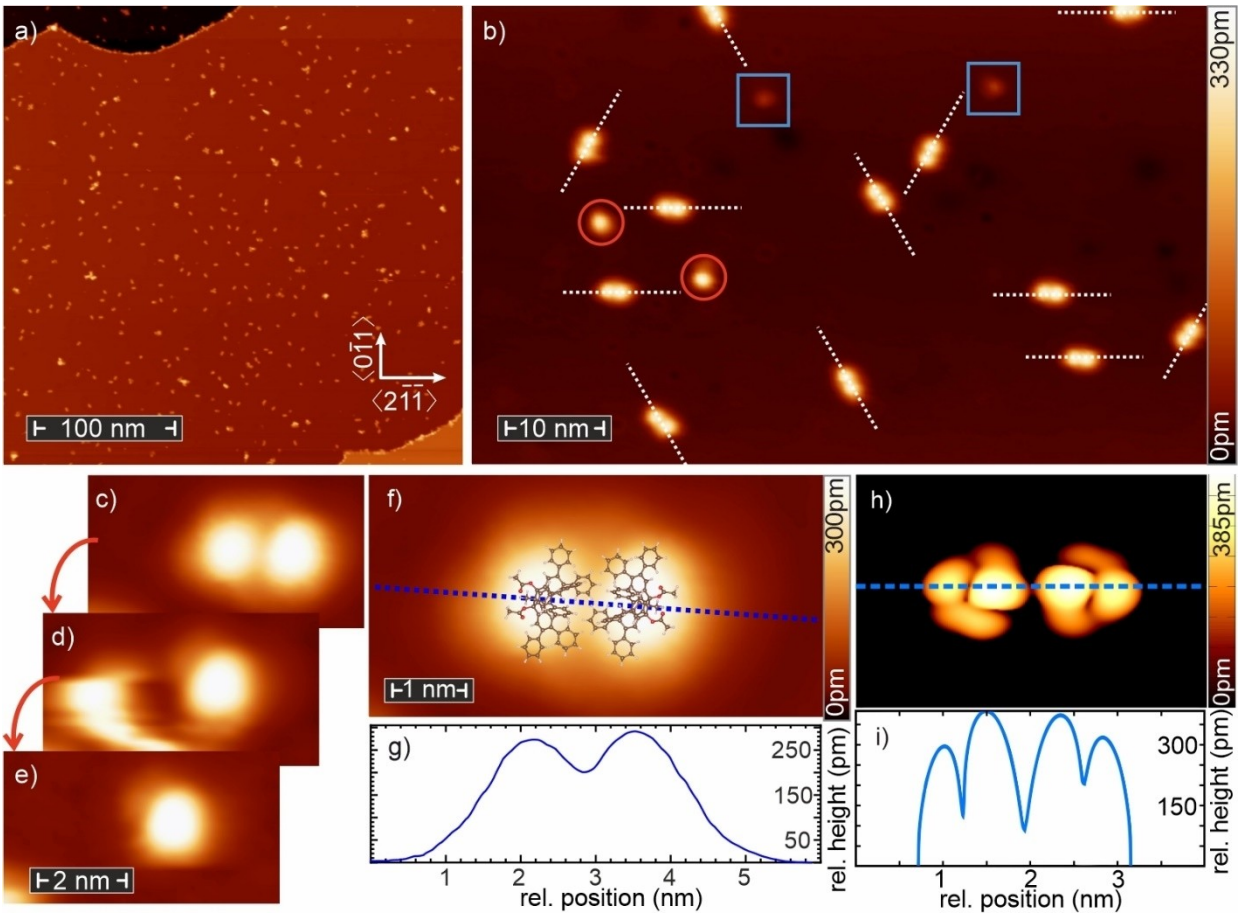

Figure 2. Low coverage deposition of Ph_6Me-TBTQ-OAc_2 on a Cu(111) surface at room temperature. a) Topography of a large terrace with monomers, dimers (both appear as small protrusions) and clusters (bright spots). Preferred adsorption at crystals step edges can be observed in the upper left and lower right corner. b) Zoom-in of several dimers and two monomers (red circles). The two indistinct protrusions in the upper part correspond to crystal defects (blue squares). As marked by dashed lines, the dimers arrange along the $\langle 2\bar{1}\bar{1}\rangle$ directions. A subtle tilt out of this orientation can be explained by shifts in the exact adsorption position on the crystal lattice. c)–e) Single-molecule STM tip manipulation: starting with a dimer c), the molecule on the left has been removed d), resulting in a monomer e). f) Enlarged topography of a dimer with the orientation of the two molecules obtained from DFT calculations. g) Height profile of the dimer measured at the dashed line in f). The inter-molecular distance is $d_{di=}(1.3\pm0.2)$ nm. h) Calculated STM image based on DFT for the structurally optimized molecule dimer on Cu(111). (i) Line profile along the blue dashed line indicated in h). STM scan parameters a)–c),e),f): $U=0.5$ V, $I=50$ pA; d): $U=0.05$ V, $I=50$ pA.

in the mass spectrometer (cf. Supporting Information). The observed dimeric structures are promoted by the existence of intermolecular π-π and C=C···H interactions.

Density functional theory (DFT) calculations on the structurally relaxed dimer reveal that each molecule binds, with two phenyl rings as well as two remaining OAc groups, flat to the surface (for computational details see the Supporting Information), whereas the third OAc group has probably been cleaved off during the evaporation process (cf. Supporting Information). The resulting calculated dimer arrangement is shown in Figure 2h where the height profile in (i) is taken along the dashed blue line. The measured and calculated line profiles deviate somewhat in extent and resolution. However, the calculations neglect the broadening of the signal due to the extended probe tip, resulting in much sharper features in the calculations.

By increasing the deposited amount on the clean substrate, molecules start to self-assemble in highly ordered structures. For example, in accordance with the dimeric model presented in Figure 2, we find elongated molecular dimer chains at a slightly enhanced coverage (see Figure S3). In addition, on-surface reactions can be observed which drastically change the appearance of these assemblies upon deposition at different substrate temperatures T_S. In the following, we analyze in detail the temperature-dependent self-assembly of the resulting TBTQ's for a coverage of (0.6 ± 0.1) monolayers. In the temperature range of RT $< T_S <$ 393 K, honeycomb lattices form islands several tens to hundreds of nanometer wide, as shown in Figure 3a. Beside these dominating structures, smaller islands with a different molecular arrangement can be found (blue arrows), surrounded by unordered molecular clusters. The honeycomb structure appears in two orientations, as highlighted by the

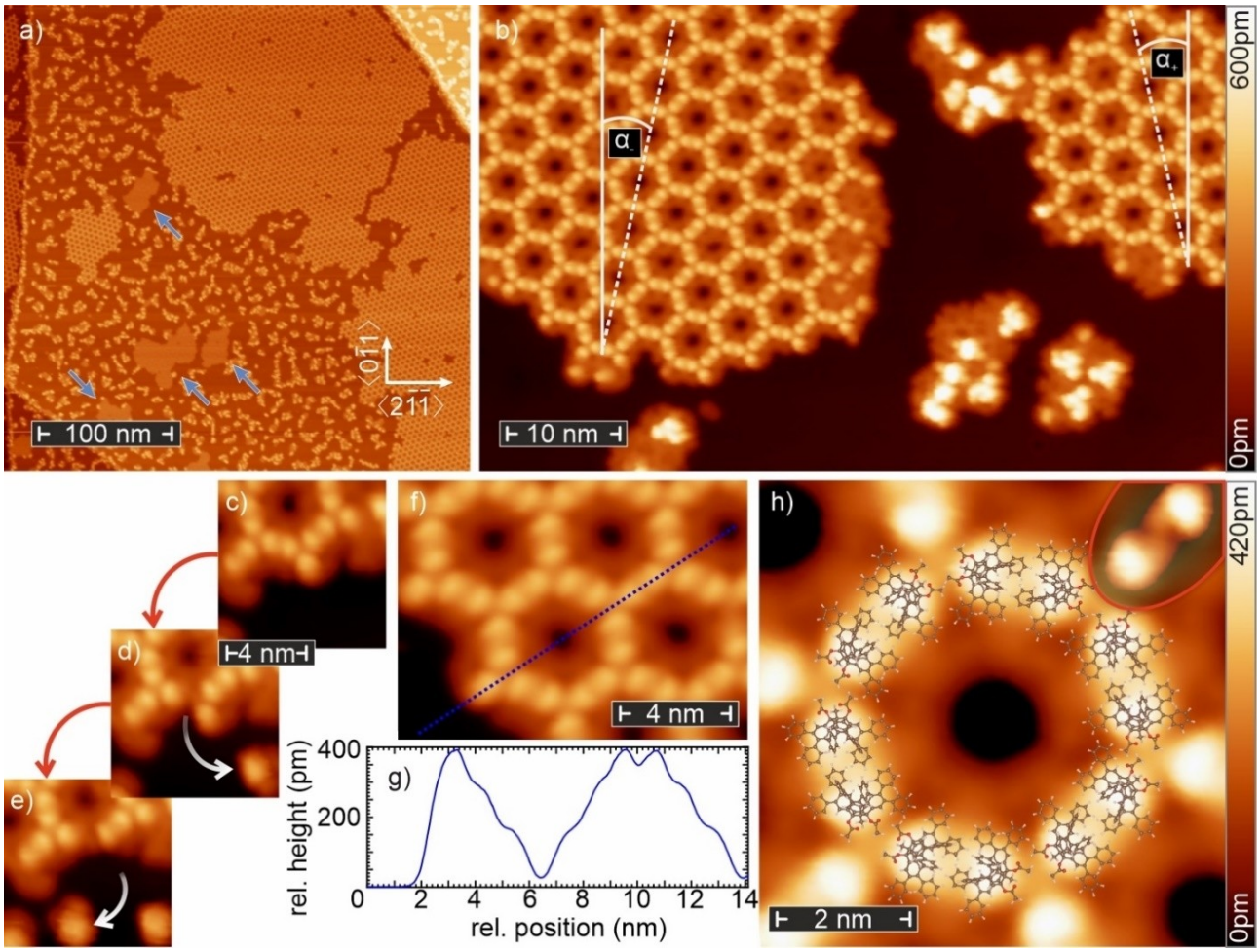

Figure 3. STM data of (0.6 ± 0.1) monolayers of Ph_6Me-TBTQ-OAc_2 on Cu(111) deposited at $T_S \approx 363$ K. a) Large islands with molecules in a honeycomb superstructure can be observed. A few small islands in an intermediate state (blue arrows) and molecular clusters are also observed. b) Enlarged scan of the two phases found for the honeycomb superstructure. The tilt of $\alpha_{+(-)=} + (-)(13 \pm 2)^\circ$ for the right (left) island towards the high symmetry axes is highlighted. At the edges of the islands, unfinished honeycombs can be observed. c)–e) Single-molecule STM-induced manipulation: Starting with an intact structure c), two molecules are removed one after the other d)–e). f) Topography of an island edge where a height profile shown in g) is taken along the dashed line. The lattice constant for the honeycomb unit cell is $a_{hoc=}$(4.4 ± 0.2) nm. h) Enlarged scan of the honeycomb with the proposed molecular arrangement. Due to the handedness of the molecules, an intra-dimer S-shape can be observed, as highlighted by the enhanced contrast (red frame). STM parameters: $U = 1$ V, $I = 50$ pA.

scan in Figure 3b, tilted by $\alpha_{+(-)=}+(-)(13\pm2)^\circ$ (dashed lines) from one of the $\langle 0\bar{1}1\rangle$ directions of the Cu substrate (solid lines). Again, by removing two molecules one-by-one from the honeycomb ring (white arrows) by means of single-molecule manipulation, we confirm that each protrusion depicts a single molecule. The height profile across the edge of an island (dashed line in Figure 3f) is given in Figure 3g. The corrugation amounts to ≈400 pm, i.e., ≈100 pm more than for the dimer, whereas the inter-molecular distance is reduced to $d_{hoc=}(1.15\pm0.1)$ nm. This indicates a reduced squeezing of the bowl in comparison to isolated dimers, which can be explained by an increased intermolecular interaction in the honeycomb arrangement. The lattice constant of the honeycomb unit cell was determined to be $a_{hoc=}(4.4\pm0.2)$ nm.

Based on these findings, we propose the molecular arrangement depicted in Figure 3h: Each edge of the honeycomb consists of a dimer. The methyl groups are pointing towards the corners, while the TBTQ bowls are facing towards each other. Close inspection of the α_- domain in Figure 3h reveals an S-shape in the connecting part of each dimer, highlighted by the inset with an enhanced contrast (red frame). The direction of this feature mirrors an enantiomeric ς-shape for the α_+ domain (see Figure S4). Therefore, we conclude that each domain contains enantiomers of only one handedness, inducing the specific rotation of the domains towards the high-symmetry axes.

By increasing the substrate temperature to 393 K $< T_S <$ 440 K, a change in the cluster appearance can be observed (Figure 4). Instead of a honeycomb lattice, islands with dimensions of tens to hundred nanometers appear in an intermediate structure (Figure 4a), which were already observed as a minor component at a lower substrate temperature (see Figure 3a, blue arrows). The zoom-in in Figure 4b

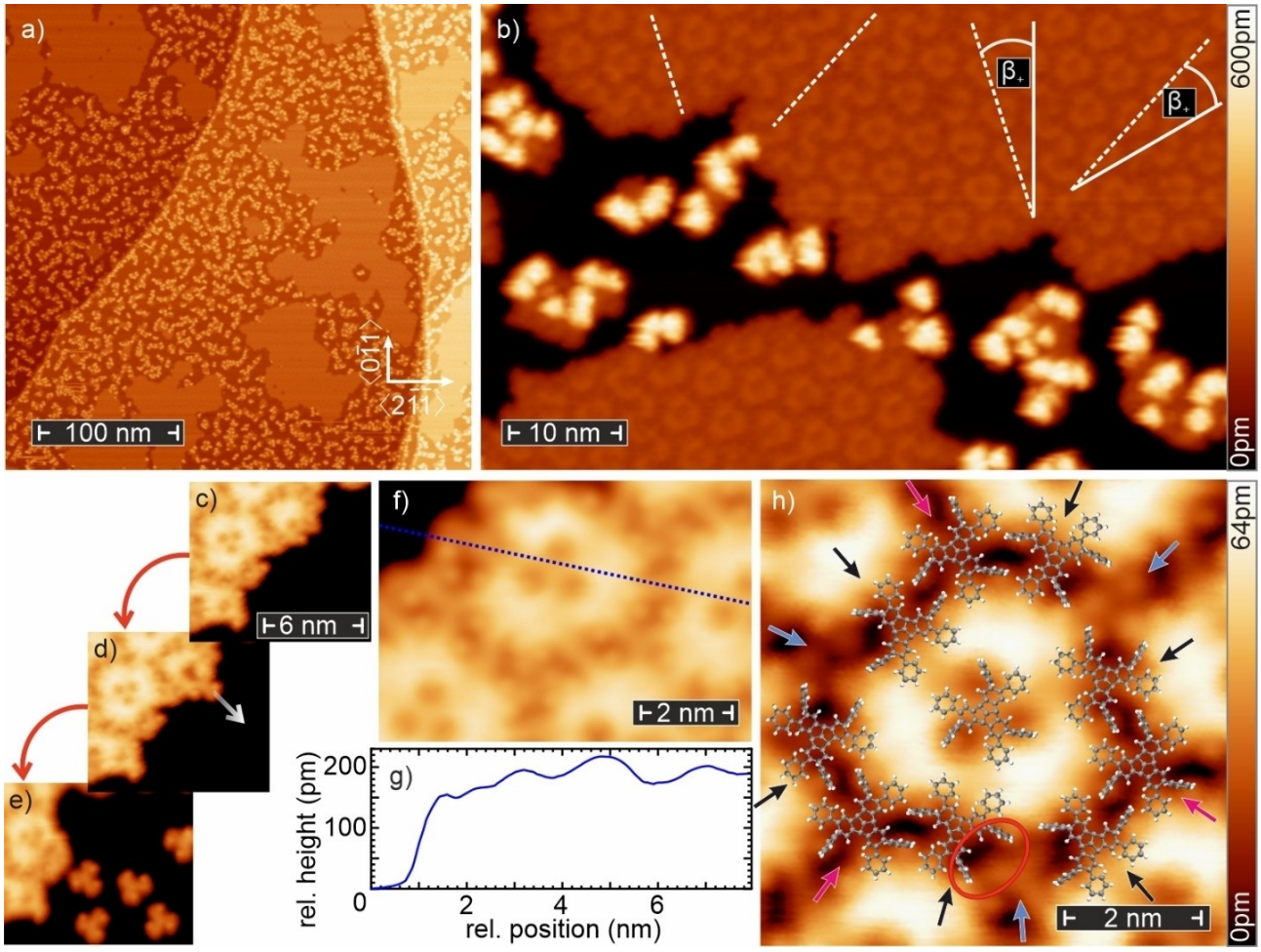

Figure 4. STM data of Ph_6-TBTQ (at 0.6 ± 0.1 monolayers) on Cu(111) deposited at T_S ≈393 K. a) Besides numerous unordered clusters, large islands with a superstructure of trigonal symmetry are observed. b) High resolution STM scan of two islands. Two rotational domains tilted by $\beta_{+=}+(18\pm2)^\circ$ from one of the $\langle 0\bar{1}1\rangle$ directions and separated by domain boundaries are indicated. c)–e) Detachment of ve molecules by STM-induced manipulation. f) Detailed STM image of the trigonal superstructure at the island edge. The height profile taken along the dashed line is shown in g). The lattice constant of the trigonal unit cell is $a_{tri=}(4.3\pm0.2)$ nm. h) High resolution scan of the trigonal lattice with the proposed molecular arrangement. In the center, as well as on three corners, a symmetrical triskelion-like molecule is observed (red arrows), whereas six of the molecules on the edges show a broken C_3-symmetry (black arrows) with two tilted phenyl rings pointing to corners not occupied by TBTQ molecules (red ellipse). The spherical protrusions (blue arrows) in three corners are assigned to methyl groups. STM parameters: $U=1$ V, $I=50$ pA.

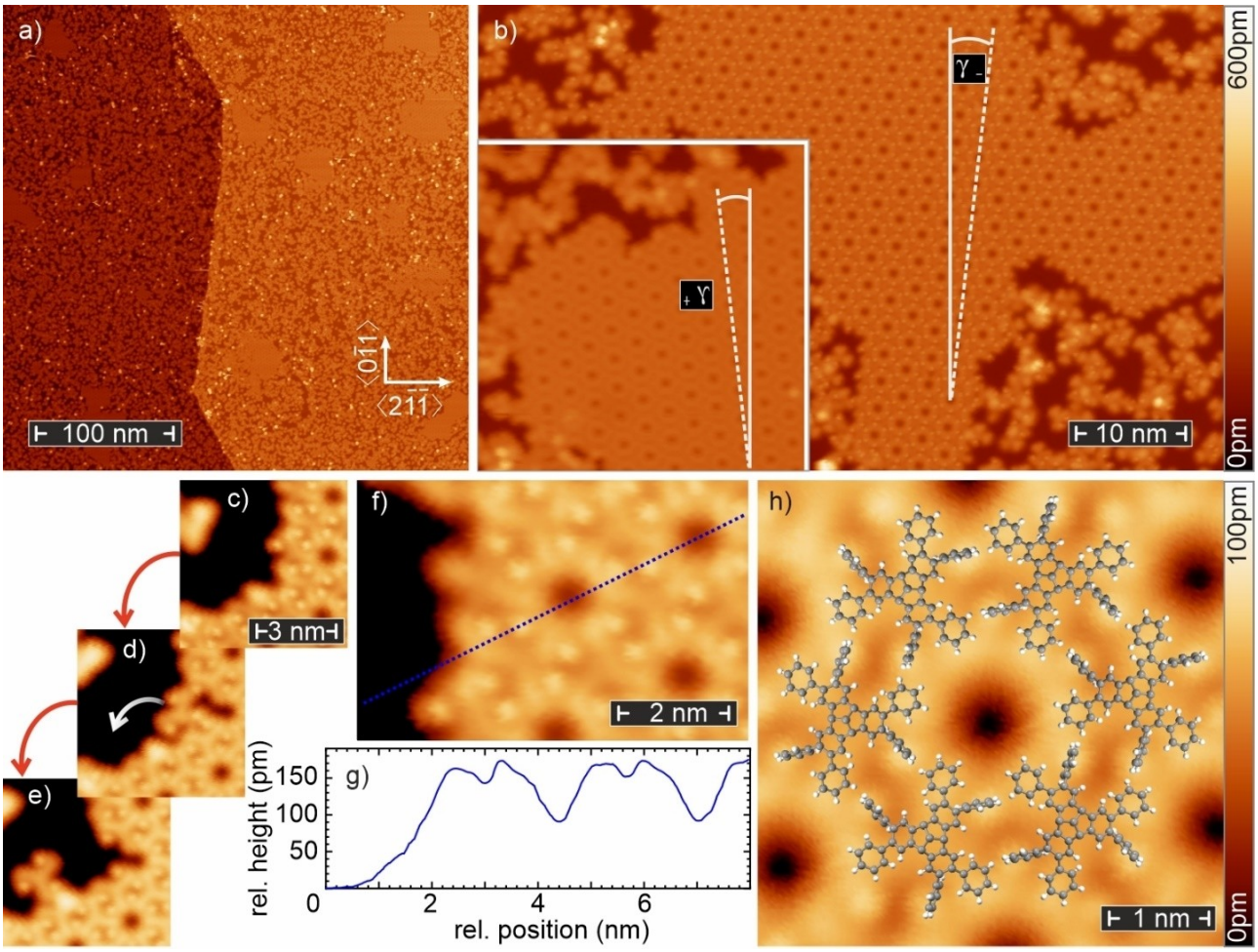

Figure 5. STM data of (0.6 ± 0.1) monolayers of Ph_6-TBTQ on Cu(111) deposited at $T_S \approx 468$ K. a) Several islands (≈50 nm across) are observed, while unordered molecules cover large areas. b) Within these islands a hexagonal superstructure is observed which, in this case, is tilted by $\gamma_{--} = -(6 \pm 2)°$ with respect to the substrate's $\langle 0\bar{1}1 \rangle$ direction. c)–e) Single-molecule manipulation: one C_3-symmetric molecule is dragged out of the edge of the hexagonal superstructure in two steps. f) High resolution STM image of the hexagonal superstructure. g) Height profile measured along the line in f). The lattice constant of the hexagonal unit cell is $a_{hex=} (2.4 \pm 0.2)$ nm. h) High resolution scan of the hexagonal lattice with a sketch of the proposed arrangement of flat-lying, triskelion-like molecules. STM parameters: $U = 1$ V, $I = 50$ pA.

reveals that these islands exhibit an equiangular hexagonal superstructure with a trigonal symmetry. Two orientations of islands rotated by $\beta_{+(-)=} + (-)(18 \pm 2)°$ from the substrate's $\langle 0\bar{1}1 \rangle$ high symmetry directions can be observed (see Figure S5). For each of these orientations, two domains can be distinguished which are rotated by 60° with respect to one another (dashed white lines in Figure 4b).

By means of single-molecule manipulation, five molecules were removed from the rim of an island, as shown in Figures 4c–e. In doing so, we find that the appearance of a single molecule changes to a three-armed, triskelion-like structure with one single dot located at each arm (see Figure S8 for detailed images). In agreement with results obtained for terphenyl derivatives,[31] this appearance is assigned to a flat lying TBTQ core with three phenyl rings oriented parallel to the surface representing the arms, whereas the dots correspond to the remaining phenyl moieties that are tilted out of the molecular plane (see structure in Figure 1c)), similar to the structure observed in the crystal. Within this structure, we observe four nonequivalent configurations, two of which exhibit a broken C_3 symmetry (see Figure S8).

It is noteworthy that the appearance of the molecules is rather flat in the center, as confirmed by the height profile in Figure 4g, taken along the dashed line in Figure 4f. It reveals a lattice constant of $a_{tri=} (4.3 \pm 0.2)$ nm and a corrugation of only 220 pm. The shallow corrugation suggests that there are no groups pointing out of the surface plane, in contrast to the previously observed Me-TBTQ.[26] Therefore, we assume that the two remaining OAc groups as well as the CH_3 group have been cleaved off at this elevated substrate temperature. Such on-surface cleavage is also supported by the signals observed by mass spectrometry (cf. Supporting Information) and has been observed previously.[32,33] In addition, as marked by blue arrows in Figure 4h, we find round protrusions which, in accordance with several publications,[34–37] are assigned to

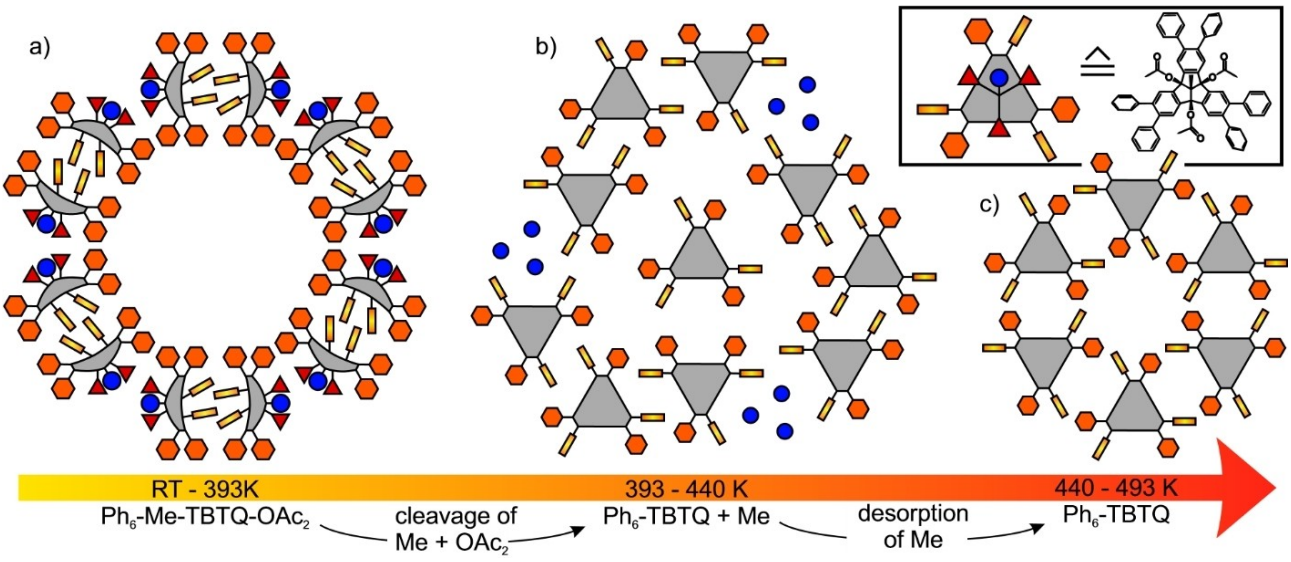

Figure 6. Evolution of the on-surface reaction of Ph_6–Me-TBTQ-OAc_3 (**1**) with rising substrate temperature and the resulting self-assembly. The inset on the top right shows the structural formula (right) and a scheme abstracting the important groups (left) of **1**: central TBTQ core (grey); phenyl rings (orange in-plane/yellow out-of-plane); CH_3 group (blue); OAc groups (red). a) Honeycomb structure consisting of twelve Ph_6–Me-TBTQ-OAc_2 molecules lying sideways, which are arranged as bowl-to-bowl facing dimers on each edge of the hexagon. b) At intermediate temperatures, a trigonal structure of ten almost flat-lying Ph_6-TBTQ is observed. c) At high temperatures, CH_3 groups detach from the surface, allowing for a hexagonal, highly-dense arrangement of six Ph_6-TBTQ.

CH_3 groups. Notably, Kuck et al. observed the cleavage of the central methyl group of Me-TBTQ at elevated temperatures in the gas phase and inferred the formation of a radical species.[27] Therefore, it can be assumed that the formation of a Ph_6-TBTQ leads to an unsaturated core which interacts strongly with the metal substrate for stabilization.[38] Our DFT calculations indeed show a significant charge transfer from the metal substrate to the molecule of around 0.05 e/atom and an almost flat adsorption configuration in which three phenyl rings are in the plane of the molecule and three are rotated 30° out of this plane (for details see Figures S12 and S13). Such electron transfer can be seen in the light of earlier investigations of the acepentalene molecule (the core structure of the Ph_6-TBTQ fragment), in which a significant electron affinity of this structure was considered.[39]

Combining these results, we predict the arrangement of single molecules in the trigonal structure presented in Figure 4h. C_3-symmetric molecules are located in the center and in three corners (red arrows). Six molecules with a broken C_3 symmetry are located on the short and long edges of the unit cell (black arrows). Each of these molecules is rotated such that two out-of-plane phenyl rings are facing towards a corner not occupied by a TBTQ, as exemplarily highlighted by a red circle. Three cleaved methyl groups are located at these edges (blue arrows). For better visibility, gas phase calculations of Ph_6-TBTQ with fully in-plane and out-of-plane rotated phenyl rings are shown.

At elevated temperatures of $440\ K < T_S < 493\ K$, islands about 50 nm in size (Figure 5a) appear in a now hexagonal superstructure (Figure 5b). We observe two orientations that are tilted by $\gamma_{+(-)=} + (-)(6 \pm 2)°$ (dashed line) from one of the $\langle 0\bar{1}1 \rangle$ surface directions (solid line) (cf. Supporting Information). By means of tip-induced manipulation, single C_3-symmetric molecules were extracted, as shown exemplarily in Figures 5c–e. A defined molecular handedness for each of the island orientations occurs, i.e., a (counter)clockwise orientation of the dots for $\gamma_{+(-)}$. The height profile in Figure 5g, taken along the dashed line in Figure 5f, reveals a corrugation of around 180 pm and lattice constant of $a_{hex=}(2.4 \pm 0.2)$ nm.

Based on these findings, we conclude that six C_3-symmetric molecules constitute one hexagon, as shown in Figure 5h. The reduced height as well as the absence of single spherical protrusions leads to the conclusion that the methyl groups desorb from the surface upon heating the substrate beyond a critical temperature. This assumption is further supported by the fact that: (i) the desorption process of methyl on a Cu(111) surface has been investigated in several studies at equivalent crystal temperatures of around 450 K;[40–42] and (ii) a hexagonal structure at intermediate temperatures shows the partial desorption of methyl groups (see Figure S7).

It is important to note that not only does deposition at a defined temperature result in the structures described, but that a stepwise structural transition on the same sample is also observed upon stepwise annealing. Therefore, the processes of OAc and CH_3 cleavage and desorption as well as the reorientation of the molecules from sideways to flat, accompanied by the rotation of peripheral phenyl rings, occur gradually on the surface. In a last annealing step at even higher substrate temperatures, long-range order is lost and an unordered distribution of highly symmetric, rather flat molecules covers the surface (see Figure S9).

To visualize the temperature-dependent structural evolution of the 2D porous lattices, a schematic abstraction is illustrated in Figure 6. As highlighted in Figure 6 (frame top right), the Ph_6–Me-TBTQ-OAc_3 molecule **1** (right) is drawn schematically to illustrate its important groups (left): central TBTQ core (grey); phenyl rings (orange in-plane/yellow out-of-plane); CH_3 group (blue); OAc groups (red). Upon evaporation, one of the OAc groups cleaves, which leads to an initial deposition of Ph_6–Me-TBTQ-OAc_2. Depositing at room temperature, Ph_6–MeTBTQ-OAc_2 molecules form dimers which, at higher coverage, arrange in a honeycomb lattice with a lattice constant of $a_{hoc=}(4.4\pm0.2)$ nm and a pore density of $\rho_{hoc}\approx7.9\times10^4/\mu m^2$, as shown in Figure 6a. The molecular bowls face each other, while the molecular plane stands perpendicular to the surface. Upon increasing the temperature, demethlyation as well as OAc-cleavage occur as on-surface reactions. The smaller Ph_6-TBTQ fragments preferably bind almost flat on the surface. Depending on the temperature, the flattened Ph_6-TBTQ molecules and CH_3 groups coexist in a complex transitional lattice with little to no porosity and molecules forced into a partially broken symmetry, as shown in Figure 6b. At even higher temperatures, the proposed desorption of the methyl-groups induces a self-assembly of a hexagonal lattice with lattice constant $a_{hex=}(2.4\pm0.2)$ nm and a significant higher pore density of $\rho_{hex}\approx2.7\times10^5/\mu m^2$. Hereby, the Ph_6-TBTQ fragments relax to a C_3 symmetry with low overall height and a presumably strong electronic interaction of their acepentalene-like core with the metal surface (see Figure 6c).

Conclusion

The self-assembly of the TBTQ investigated on Cu(111) surfaces is an outstanding example of the controlled creation of highly ordered networks by a C_3 symmetric molecule. Moreover, the structural properties and pore size of the 2D lattices can be controlled by the substrate temperature. Upon room temperature deposition, we find honeycomb structures which consist of intact dimers of Ph_6–Me-TBTQ-OAc_2. Heating the substrate to elevated temperatures leads to an on-surface deacetylation and demethylation, resulting in Ph_6-TBTQ formation. These molecules tend to bind flat to the substrate in order to compensate the unsaturated core by charge transfer with the underlying crystal, as confirmed by DFT calculations. In a complex intermediate structure, both Ph_6-TBTQ as well as cleaved CH_3 are observed in a trigonal arrangement. At higher temperatures, the CH_3 groups desorb from the surface, allowing for a highly ordered, flat hexagonal structure of Ph_6-TBTQ. As these structures not only evolve by deposition on a hot surface, but also subsequently by annealing of deposited layers, the on-surface reaction indeed proceeds stepwise. Thereby, the cleavage and desorption of OAc and CH_3 as well as the reorientation of the molecules from sideways to flat, accompanied by rotations of the peripheral phenyl rings, occurs gradually within a temperature range of 200 K. This detailed study of a porous 2D lattice provides fundamental understanding of structure formation and transition in on-surface reactions, paving the way towards extended, holey graphene networks with unique electronic structures.

Experimental Section

Compounds **2**, **3** and **4** were synthetized using adapted literature procedures (see Supporting Information for details and full characterization).

5: 300 mg (0.273 mmol, 1 equiv.) of hexaiodotriol **4**, was dissolved in 50 mL of dichloromethane with the help of an ultrasonic bath. Then, 9 mL of Ac_2O (0.97 mol), 15 mL of pyridine and 210 mg of DMAP were added to the solution. The resulting mixture was stirred at ambient temperature for 3 d. The solution was diluted with 300 mL of Et_2O and extracted with 2 N HCl, saturated $NaHCO_3$, distilled water and brine two times each (800 mL total volume). The organic phase was dried over $MgSO_4$ and the solvent was removed under reduced pressure. The extracted product was recrystallized using dichloromethane, and **5** was obtained as a colorless powder (241 mg, 72%), $\mathbf{F_p}$: 330 °C (decomp.), $\mathbf{R_f}$: 0.44 (cyclohexane/ ethyl acetate 2:1), **^{1}H NMR** (400 MHz, DMSO-d_6): $\delta=7.90$ (6H, s, 8/5/4/1/12/9-H), 2.16 (9H, s, C(O)–CH_3), 1.45 (3H, s, CH_3) ppm, **^{13}C NMR** (100 MHz, $CDCl_3$): $\delta=$ 169.69 (C_q, –OC(O)Me), 142.35 (C_t, C-8/5/4/1/12/9), 133.90 (C_q, C-8a/4c/4a/12c/12a/8a), 110.02 (C_q, C-7/6/3/2/10/11), 94.53 (C_t, C-4b/8b/12b), 30.97 (C_q, C-12d), 21.79 (C_p, C(O)–CH3), 12.39 (C_t, C(12d)CH_3) ppm, **FTIR**: $\tilde{\upsilon}=3012$ (w, ν(C–H_{arom})), 2969 (w, ν (C–H_{arom})), 2945 (w, ν (C–H_{arom})), 2902 (w), 2889 (w), 2827 (w), 2191 (w), 2164 (w), 2141 (w), 1743 (s), 1624 (w), 1583 (w), 1444 (m, ν(C=C_{arom})), 1367 (m, $\delta(CH_3)$), 1348 (m), 1277 (m), 1213 (vs), 1082 (m), 1053 (s), 1007 (s), 984 (s), 957 (m), 899 (m), 870 (s), 756 (w), 721 (w), 681 (m), 617 (m) cm^{-1}, **UV/Vis** (CH_2Cl_2, lg ε): $\lambda_{max}=$ 306 (0.26), 296 (0.26), 252 (2.06), 238 (2.02) nm, **HRMS** (APCI, pos): calc. for [$C_{29}H_{18}I_6O_6+H$] m/z 1224.54, [$C_{27}H_{15}I_6O_4^+$] m/z 1164.52, found [M^+-OAc] m/z 1164.5224, **EA**: calc**. C**: 28.46; **H**: 1.48; **I**: 62.21; **O**: 7.84; found **C**: 28.36; **H**: 1.70.

1: 160.0 mg, 1.0 equiv., 0.131 mmol) of **5**, 0.407 g (34 equiv., 4.44 mmol) of phenyl boronic acid, 0.107 g (4.16 equiv., 0.543 mmol) of PPh_3 and 0.81 g (14.4 mmol) of KOH were dissolved in a nitrobenzene (37.5 mL) and water (12.5 mL) mixture and placed in a Schlenk flask under nitrogen atmosphere. The solution was degassed three times, then the $Pd(dba)_2$ (25 mg) was added. The resulting mixture was degassed once more and heated to reflux overnight. The resulting reaction mixture was cooled to room temperature and subsequently diluted with 200 mL of Et_2O. The mixture was extracted with 2 M KOH, 0.1 M HCl, dist. H_2O and brine solutions. The organic phase was dried over $MgSO_4$ and the solvent was removed in vacuo. The crude product was purified with flash column chromatography (4:1:1, CH/EA/DCM). Further purification for STM investigations was performed by reversed phase HPLC (Reprosil C-18-PQ-JASCO semi preparative column, 5 μm, 250 mm × 10 mm) using acetonitrile as eluent. **1** was isolated as a cream-colored crystalline solid (100 mg, 0.108 mmol, 83%), $\mathbf{F_p}$: 248–252 °C, R_f: 0.54 (cyclohexane/ ethyl acetate 2:1), **^{1}H NMR** (600 MHz, DMSO-d_6): $\delta=7.83$ (s, 6H, 1/4-H), 7.24–7.17 (m, 18H, 3′/4′/5′- H), 7.03-7.01(dt, $J=1.910$ Hz, 12H, 2′/6′-H), 2.16 (s, 9H, 4b2/8b2/12b2-H), 1.56 (3H, s, CH_3) ppm, **^{13}C NMR** (600 MHz, DMSO-d_6): $\delta=169.66$ (C_q, –OC(O)Me, C-4b1/8b1/12b1), 141.79 (C_q, C-1′), 140.97 (C_q, C-8a/4c/4a/12c/12a/8a), 140.55 (C_q, C-7/6/3/2/10/11), 128.02 (C_t, C-3′,4′), 126.82 (C_t, C-5′), 125.58 (C_t, C-2′, 6′), 125.45 (C_t, C-1/4/5/8/9/12), 95.95 (C_q, C-4b/8b/12b), 76.94 (C_q, C-12d), 21.72 ((O)CH_3, C-

4b2/8b2/12b2), 12.28 (C_p, C(12d)CH_3) ppm, **FTIR**: $\tilde{\upsilon}$ = 3056 (w, ν(C–H_{arom})), 3027 (w, ν(C–H_{arom})), 2921 (w, ν(C–H_{arom}), 2848 (m, ν(C–H_{arom})), 1745 (s, ν(C=O)), 1600 (w, ν(C=C_{arom})) 1571 (w, ν(C-, C=C_{arom})), 1477 (m), 1446 (m) 1369 (m, δ(CH_3)), 1326 (w), 1213 (s, ν(C–C=O)), 1176 (m), 1074 (w), 1037 (s), 1018 (s), 983 (s), 946 (m), 902 (m), 879 (m), 813 (w), 763 (s), 698 (s), 640 (w), 609 (w) cm^{-1}, **UV/Vis** (CH_2Cl_2, lgε): λmax = 302 (0.47), 256 (2.92), 231 (2.41) nm, HRMS (APCI, +): calc. for [$C_{65}H_{48}O_6$ + H] m/z 925.35, found m/z 925.3414, EA: calc. C: 84.39; H: 5.23; O: 10.38 found C: 84.33 H: 5.51.

The **STM measurements** were performed under ultra-high vacuum (UHV) conditions (base pressure $p \leq 1 \times 10^{-10}$ mbar). Sample preparation and analysis were performed in two separate chambers. The Cu(111) single crystal was prepared by multiple cycles of 30 min Ar^+ sputtering at an ion energy of 1 keV and a temperature of 650 K followed by annealing at 750 K for 15 min. Ph_6-Me-TBTQ-OAc_3 molecules (**1**) were deposited onto the clean Cu(111) surface by a four cell Dodecon evaporator with a filament-heated crucible. During evaporation, the crystal was tempered by a resistive heater, while the temperature T_S was measured with a thermocouple directly attached to the manipulator. Upon *in vacuo* transfer to the other UHV chamber, the samples were loaded into the sample slot of a home-built low-temperature scanning tunnelling microscope (STM) with an operation temperature of about 4.5 K. STM probe tips were electrochemically etched from polycrystalline tungsten wires and gently dipped into the Cu(111) substrate for tip conditioning. Manipulation of single molecules was performed with the STM tip at tunnelling parameters of U = 20.50 mV, I = 0.5–50 nA.

Deposition Number 2093789 (for **1**) contains the supplementary crystallographic data for this paper. These data are provided free of charge by the joint Cambridge Crystallographic Data Centre and Fachinformationszentrum Karlsruhe Access Structures service.

Acknowledgements

A.K. acknowledges the support by the Deutsche Forschungsgemeinschaft (GRK 2112) and the University of Stuttgart. A.K. and T.B.M acknowledge support by the Julius-Maximilians-Universität Würzburg and S.T. thanks the Graduate School of Science and Technology and DAAD-STIBET for a scholarship. Support by the Dresden-Würzburg Center for Topological Quantum Matter Research (ct.qmat) is gratefully acknowledged by M.B. S.J.H. S.H. thanks the Norddeutscher Verbund für Hoch- und Höchstleistungsrechnen (HLRN) for providing computational resources and the Deutsche Forschungsgemeinschaft (DFG, German Research Foundation) for financial support via project no. 445697818. Open Access funding enabled and organized by Projekt DEAL.

Conflict of Interest

The authors declare no conflict of interest.

Data Availability Statement

The data that support the findings of this study are available in the supplementary material of this article.

Keywords: 2D lattices · nanostructures · on surface chemistry · scanning tunnelling microscopy · triquinacenes

[1] D. P. Goronzy, M. Ebrahimi, F. Rosei, A. Arramel, Y. Fang, S. De Feyter, S. L. Tait, C. Wang, P. H. Beton, A. T. S. Wee, P. S. Weiss, D. F. Perepichka, *ACS Nano* **2018**, *12*, 7445–7481.
[2] R. Sekiya, T. Haino, *Chem. Rec.* **2022**, *22*, e202100257.
[3] A. R. Brill, E. Koren, G. de Ruiter, *J. Mater. Chem. C* **2021**, *9*, 11569–11587.
[4] J. Zha, M. Luo, M. Ye, T. Ahmed, X. Yu, D.-H. Lien, Q. He, D. Lei, J. C. Ho, J. Bullock, K. B. Crozier, C. Tan, *Adv. Funct. Mater.* **2022**, *32*, 2111970.
[5] M. Zeng, Y. Xiao, J. Liu, K. Yang, L. Fu, *Chem. Rev.* **2018**, *118*, 6236–6296.
[6] A. Kumar, K. Banerjee, P. Liljeroth, *Nanotechnology* **2017**, *28*, 082001.
[7] G. Poluektov, T. J. Keller, A. Jochemich, A. Krönert, U. Müller, S. Spicher, S. Grimme, S.-S. Jester, S. Höger, *Angew. Chem.* **2021**, *133*, 27470–27476; *Angew. Chem. Int. Ed.* **2021**, *60*, 27264–27270.
[8] J. Hieulle, S. Castro, N. Friedrich, A. Vegliante, F. R. Lara, S. Sanz, D. Rey, M. Corso, T. Frederiksen, J. I. Pascual, D. Peæa, *Angew. Chem.* **2021**, *133*, 25428–25433; *Angew. Chem. Int. Ed.* **2021**, *60*, 25224–25229.
[9] Q. Chen, M. Baumgarten, M. Wagner, Y. Hu, I. C.-Y. Hou, A. Narita, K. Müllen, *Angew. Chem.* **2021**, *133*, 11400–11404; *Angew. Chem. Int. Ed.* **2021**, *60*, 11300–11304.
[10] W. Ran, A. Walz, K. Stoiber, P. Knecht, H. Xu, A. C. Papageorgiou, A. Huettig, D. Cortizo-Lacalle, J. P. Mora-Fuentes, J. A. Mateo-Alonso, H. Schlichting, R. Reichert, J. V. Barth, *Angew. Chem.* **2022**, *134*, e202111816; *Angew. Chem. Int. Ed.* **2022**, *61*, e202111816.
[11] R. E. Blackwell, F. Zhao, E. Brooks, J. Zhu, I. Piskun, S. Wang, A. Delgado, Y.-L. Lee, S. G. Louie, F. R. Fischer, *Nature* **2021**, *600*, 647–652.
[12] K. Biswas, J. I. Urgel, K. Xu, J. Ma, A. Sánchez-Grande, P. Mutombo, A. Gallardo, K. Lauwaet, B. Mallada, B. de la Torre, A. Matěj, J. Gallego, R. Miranda, P. Jelínek, X. Feng, D. Écija, *Angew. Chem.* **2021**, *133*, 25755–25760; *Angew. Chem. Int. Ed.* **2021**, *60*, 25551–25556.
[13] T. G. Lohr, J. I. Urgel, K. Eimre, J. Liu, M. Di Giovannantonio, S. Mishra, R. Berger, P. Ruffieux, C. A. Pignedoli, R. Fasel, X. Feng, *J. Am. Chem. Soc.* **2020**, *142*, 13565–13572.
[14] J. I. Urgel, M. Di Giovannantonio, Y. Segawa, P. Ruffieux, L. T. Scott, C. A. Pignedoli, K. Itami, R. Fasel, *J. Am. Chem. Soc.* **2019**, *141*, 13158–13164.
[15] T. Jasper-Tönnies, M. Gruber, S. Ulrich, R. Herges, R. Berndt, *Angew. Chem.* **2020**, *132*, 7074–7083; *Angew. Chem. Int. Ed.* **2020**, *59*, 7008–7017.
[16] L. He, C.-F. Ng, Y. Li, Z. Liu, D. Kuck, H.-F. Chow, *Angew. Chem.* **2018**, *130*, 13823–13827; *Angew. Chem. Int. Ed.* **2018**, *57*, 13635–13639.
[17] S. Ivanova, E. Köster, J. J. Holstein, N. Keller, G. H. Clever, T. Bein, F. Beuerle, *Angew. Chem.* **2021**, *133*, 17595–17604; *Angew. Chem. Int. Ed.* **2021**, *60*, 17455–17463.
[18] P. Wagner, F. Rominger, W.-S. Zhang, J. H. Gross, S. M. Elbert, R. R. Schröder, M. Mastalerz, *Angew. Chem.* **2021**, *133*, 8978–8986; *Angew. Chem. Int. Ed.* **2021**, *60*, 8896–8904.
[19] H.-W. Ip, Y. Li, D. Kuck, H.-F. Chow, *J. Org. Chem.* **2021**, *86*, 5546–5551.
[20] L. Ueberricke, B. Punja Benke, T. Kirschbaum, S. Hahn, F. Rominger, U. H. F. Bunz, M. Mastalerz, *Chem. Eur. J.* **2021**, *27*, 2043–2049.
[21] A. Dhara, F. Beuerle, *Synthesis* **2018**, *50*, 2867–2877.
[22] P. Wagner, F. Rominger, M. Mastalerz, *Angew. Chem.* **2018**, *130*, 11491–11494; *Angew. Chem. Int. Ed.* **2018**, *57*, 11321–11324.
[23] W. Greschner, B. Neumann, H.-G. Stammler, H. Gröger, D. Kuck, *Angew. Chem.* **2015**, *127*, 13968–13972; *Angew. Chem. Int. Ed.* **2015**, *54*, 13764–13768.
[24] J. G. Brandenburg, S. Grimme, P. G. Jones, G. Markopoulos, H. Hopf, M. K. Cyranski, D. Kuck, *Chem. Eur. J.* **2013**, *19*, 9930–9938.
[25] Y. Kirchwehm, A. Damme, T. Kupfer, H. Braunschweig, A. Krueger, *Chem. Commun.* **2012**, *48*, 1502–1504.
[26] M. Vogt, R. Buschmann, S. Toksabay, M. Schmitt, M. Schwab, M. Bode, A. Krueger, *J. Phys. Chem. C* **2019**, *123*, 5469–5478.
[27] D. Kuck, *Angew. Chem.* **1984**, *96*, 515–516; *Angew. Chem. Int. Ed.* **1984**, *23*, 508–509.
[28] D. Beaudoin, F. Rominger, M. Mastalerz, *Synthesis* **2015**, *47*, 3846–3848.
[29] D. Kuck, A. Schuster, R. A. Krause, J. Tellenbröker, C. P. Exner, M. Penk, H. Bögge, A. Müller, *Tetrahedron* **2001**, *57*, 3587–3613.

[30] G. Höfle, W. Steglich, H. Vorbrüggen, *Angew. Chem.* **1978**, *90*, 602–615; *Angew. Chem. Int. Ed.* **1978**, *17*, 569–583.
[31] Q. Fan, S. Werner, J. Tschakert, D. Ebeling, A. Schirmeisen, G. Hilt, W. Hieringer, J. M. Gottfried, *J. Am. Chem. Soc.* **2018**, *140*, 7526–7532.
[32] F. Schlütter, F. Rossel, M. Kivala, V. Enkelmann, J.-P. Gisselbrecht, P. Ruffieux, R. Fasel, K. Müllen, *J. Am. Chem. Soc.* **2013**, *135*, 4550–4557.
[33] M. Bieri, S. Blankenburg, M. Kivala, C. A. Pignedoli, P. Ruffieux, K. Müllen, R. Fasel, *Chem. Commun.* **2011**, *47*, 10239–10241.
[34] M. D. Marcinkowski, M. T. Darby, J. Liu, J. M. Wimble, F. R. Lucci, S. Lee, A. Michaelides, M. Flytzani-Stephanopoulos, M. Stamatakis, E. C. H. Sykes, *Nat. Chem.* **2018**, *10*, 325–332.
[35] Y.-L. Chan, W. W. Pai, T. J. Chuang, *J. Phys. Chem. B* **2004**, *108*, 815–818.
[36] H. Yu, L. J. Webb, R. S. Ries, S. D. Solares, W. A. Goddard, J. R. Heath, N. S. Lewis, *J. Phys. Chem. B* **2005**, *109*, 671–674.
[37] W. W. Pai, Y. L. Chan, T. J. Chuang, *Chin. J. Phys.* **2005**, *43*, 212–218.
[38] D. Kuck, A. Schuster, B. Ohlhorst, V. Sinnwell, A. de Meijere, *Angew. Chem.* **1989**, *101*, 626–628; *Angew. Chem. Int. Ed.* **1989**, *28*, 595–597.
[39] R. Haag, D. Schröder, T. Zywietz, H. Jiao, H. Schwarz, P. von Ragué Schleyer, A. de Meijere, *Angew. Chem.* **1996**, *108*, 1413–1416; *Angew. Chem. Int. Ed.* **1996**, *35*, 1317–1319.
[40] T. Chuang, Y. Chan, P. Chuang, R. Klauser, *J. Electron Spectrosc. Relat. Phenom.* **1999**, *98–99*, 149–173.
[41] J. L. Lin, B. E. Bent, *J. Phys. Chem.* **1993**, *97*, 9713–9718.
[42] C.-M. Chiang, B. E. Bent, *Surf. Sci.* **1992**, *279*, 79–88.
[43] H.-Y. Gao, H. Wagner, P. A. Held, S. Du, H.-J. Gao, A. Studer, H. Fuchs, *Appl. Phys. Lett.* **2015**, *106*, 081606.

Manuscript received: October 12, 2022
Accepted manuscript online: November 8, 2022
Version of record online: January 4, 2023